JOURNAL OF CHEMICAL INFORMATION AND MODELING

Article

pubs.acs.org/jcim

Computational Study on the Drug Resistance Mechanism against HCV NS3/4A Protease Inhibitors Vaniprevir and MK-5172 by the Combination Use of Molecular Dynamics Simulation, Residue Interaction Network, and Substrate Envelope Analysis

Weiwei Xue,[†] Yihe Ban,[†] Huanxiang Liu,[‡] and Xiaojun Yao*[,†,§]

[†]State Key Laboratory of Applied Organic Chemistry, Department of Chemistry, Lanzhou University, Lanzhou 730000, China

[‡]School of Pharmacy, Lanzhou University, Lanzhou 730000, China

[§]Key Lab of Preclinical Study for New Drugs of Gansu Province, Lanzhou University, Lanzhou 730000, China

Supporting Information

ABSTRACT: Hepatitis C virus (HCV) NS3/4A protease is an important and attractive target for anti-HCV drug development and discovery. Vaniprevir (phase III clinical trials) and MK-5172 (phase II clinical trials) are two potent antiviral compounds that target NS3/4A protease. However, the emergence of resistance to these two inhibitors reduced the effectiveness of vaniprevir and MK-5172 against viral replication. Among the drug resistance mutations, three single-site mutations at residues Arg155, Ala156, and Asp168 in NS3/4A protease are especially important due to their resistance to nearly all inhibitors in clinical development. A detailed understanding of drug resistance mechanism to vaniprevir and MK-5172 is therefore very crucial for the design of novel potent agents targeting viral variants. In this work, molecular dynamics (MD) simulation, binding free energy calculation, free energy decomposition, residue interaction network (RIN), and substrate envelope analysis were used to study the detailed drug resistance mechanism of the three mutants R155K, A156T, and D168A to vaniprevir and MK-5172. MD simulation was used to investigate the binding mode for these two inhibitors to wild-type and resistant mutants of HCV NS3/4A protease. Binding free energy calculation and free energy decomposition analysis reveal that drug resistance mutations reduced the interactions between the active site residues and substituent in the P2 to P4 linker of vaniprevir and MK-5172. Furthermore, RIN and substrate envelope analysis indicate that the studied mutations of the residues are located outside the substrate (4B5A) binding site and selectively decrease the affinity of inhibitors but not the activity of the enzyme and consequently help NS3/4A protease escape from the effect of the inhibitors without influencing the affinity of substrate binding. These findings can provide useful information for understanding the drug resistance mechanism against vaniprevir and MK-5172. The results can also provide some potential clues for further design of novel inhibitors that are less susceptible to drug resistance.

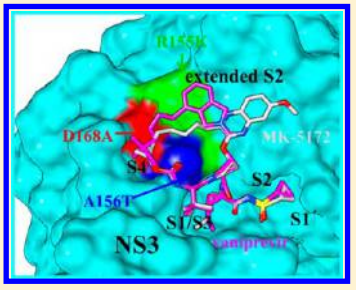

INTRODUCTION

Chronic hepatitis C virus (HCV) infects over 180 million people worldwide and is a leading cause of several chronic liver diseases.[1] At present, the standard of care for HCV patients is based on a combination of weekly injections of pegylated interferon (IFN) and daily oral doses of ribavirin. IFN acts by inducing IFN-stimulated genes (ISGs), which establish a nonvirus-specific antiviral state within the cell and ribavirin leads to upregulation of several ISGs and enhances signal transducer and activator of transcription proteins binding to DNA. However, combination therapy is expensive and associated with frequent and troublesome side effects and contraindicated in many patients.[2−5] Recently, the therapy of HCV has been greatly improved by the use of boceprevir[6] and telaprevir,[7] two approved antiviral agents specifically targeting HCV NS3/4A protease.[8]

HCV NS3/4A is a trypsin-like serine protease involved in viral polyprotein processing. The 181-residue N-terminal protease domain of the NS3 protein formed a heterodimer with the small 54-residue NS4A peptide cofactor and results in the subsequent downstream cleavage of the HCV polyprotein at the junctions between NS3/4A, NS4A/4B, NS4B/5A, and NS5A/B.[9,10] Over the past two decades, NS3/4A protease has been proven to be a very important target for anti-HCV drug design and discovery.

To date, a series of NS3/4A protease inhibitors (PIs) have been developed by structure-based drug design (SBDD). Among them, boceprevir and telaprevir were approved by U.S. Food and Drug Administration in 2011. These two molecules are linear peptidomimetic inhibitors possessing a serine trap that reversibly forms a covalent bond with the enzyme. Besides, other representative PIs currently in clinical development include the macrocyclic compounds TMC435[11] (phase III clinical trials), danoprevir[12] (phase III clinical trials), vaniprevir[13] (phase III clinical trials), and MK-5172[14] (phase II

Received: January 25, 2013
Published: June 9, 2013

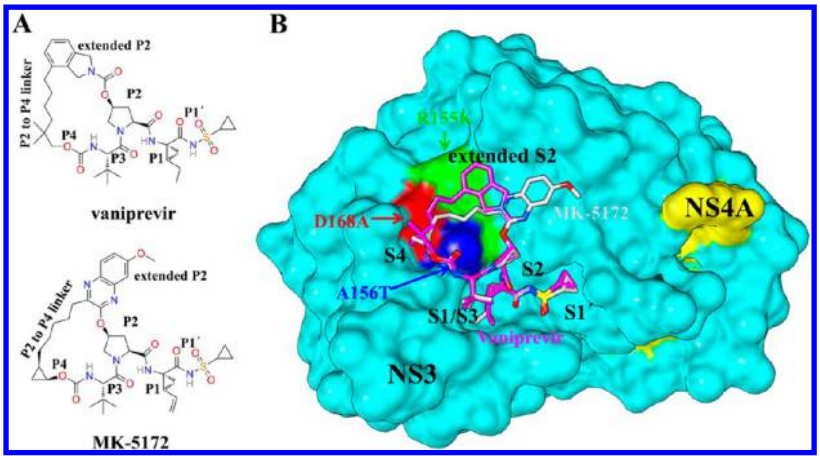

Figure 1. Structures of HCV NS3/4A protease and its inhibitors. (A) Chemical structures of vaniprevir and MK-5172. The indicated P1, P1′, P2, P3, and P4 are substrate positions from NS3/4A complex structures. (B) Crystal structure of vaniprevir and MK-5172 bound to the active site of NS3/4A protease (PDB ID code 3SU3 and 3SUD). The mutation residues which confer drug resistance are particularly labeled. The NS3 protease and NS4A cofactor peptide are distinguished in cyan and yellow surface with the selected subsites indicated. Vaniprevir and MK-5172 are shown in gray and pink stick models, respectively.

clinical trials). These drugs are direct acting antivirals (DDAs) against NS3/4A protease and represent a major breakthrough for the treatment of chronic HCV infection. However, *in vitro* experiments show that single-site mutations in NS3/4A protease could cause different levels of resistance to all PIs and reduce drug sensitivity.[15,16] In addition, the shallow catalytic site of HCV NS3/4A protease allows minor structural modifications to interfere with substrate binding.[16] Therefore, to develop potent and effective anti-HCV drugs against the viral variants, the detailed understanding about the molecular basis of drug resistance against NS3/4A PIs at the atomic level will be very urgent and important.

During the past years, molecular modeling methods such as molecular docking, molecular dynamics (MD) simulation, and binding free energy calculation have been proved to be very useful and successful in understanding the molecular basis of drug resistance to different antiviral agents. The typical success cases include the drug resistance mechanism studies against inhibitors to HIV protease, HIV reverse transcriptase (RT), HIV integrase (IN), influenza neuraminidase (NA), and HCV NS3/4A protease, etc.[17−34] MD simulation and binding free energy calculation can provide useful structural and energetic information about the interaction between the inhibitors and the targets. In addition, the resistance mutation or substitution in the drug target often affects the binding ability of drugs through influencing the residue interaction network (RIN) communication of the targets.[35−38] Recent studies have also shown that the analysis and interactive visualization of RIN of proteins will be very useful for gaining insight into complex biological interactions in the studied systems.[39,40] Substrate envelope analysis is also very helpful in understanding the drug resistance mechanism and in drug molecules mimicking the exact shape of the substrates of the protein targets. In recent years, incorporating substrate envelope hypothesis into structure-based drug design has developed a series of new HIV-1 protease inhibitors.[41−43]

In this work, on the basis of the recently determined X-ray crystal structures[44] of vaniprevir and MK-5172 (Figure 1A) in complex with the wild-type HCV NS3/4A protease and its three single-site mutations including R155K, A156T, and D168A (Figure 1B), MD simulation, binding free energy calculation, free energy decomposition, RIN, and substrate envelope analysis were used to explore the drug resistance mechanism of vaniprevir and MK-5172 to NS3/4A protease mutants. The combination use of these approaches can be effective in studying the detailed drug resistance mechanism. MD simulation is capable of revealing the binding mode for PIs with wild-type protease and its mutants. The calculated binding free energy and free energy decomposition analysis help us to understand the detailed interaction profiles of the PIs. Results reveal that the drug resistance mutations can directly or indirectly decrease the interaction contributions from the important residues; for example, in the R155K mutant complex, the contributions from residues Lys155 and Asp168 are decreased by 3.52 and 1.15 kcal/mol for vaniprevir, and the contributions from residues Tyr56, Asp81, Lys155, and Asp168 are decreased by 1.08, 0.72, 1.40, and 0.31 kcal/mol for MK-5172. In addition, RIN analysis of the complex can provide some information about the network for the residue interactions to discover the possible mechanisms of drug resistance. Furthermore, results from substrate envelope analysis demonstrate that the studied drug resistance mutations of NS3/4A are located outside the viral substrate (the viral cleavage product peptide) 4B5A envelope, thereby weakening the affinity of the vaniprevir and MK-5172 to HCV NS3/4A protease without influencing substrate binding.

MATERIALS AND METHODS

System Preparation. The initial atomic coordinates for vaniprevir and MK-5172 in complex with WT, R155K, D168A, and A156T mutant NS3/4A proteases were obtained from the RCSB Protein Data Bank (PDB ID code: 3SU3, 3SU4, 3SU5, 3SU6, 3SUD, 3SUE, 3SUF, and 3SUG, respectively).[44] The S139A protease mutant was used for crystallization of the mutant protease (PDB ID code: 3SUD).[44] In this study, the Mutagenesis module of PyMOL[45] was applied to mutate the alanine located in position 139 of the crystal structure 3SUD back to serine. The crystal structure of NS3/4A protease complexed with its peptide product 4B5A was retrieved from the Protein Data Bank (PDB ID code: 3M5N[46]). As the crystal structures of the mutant are unknown, the 3D structures of the three mutants were generated by substituting specific residues

using the wild-type model as the template. All the structures were then modeled by using the program LEaP embedded in AMBER10[47] with the standard ff03 force field[48] used for the protein, including adding all missing hydrogen atoms of the protein. The force field parameters for vaniprevir and MK-5172 were created with the use of the Antechamber program from AMBER10, using General Amber Force Field (GAFF),[78] and restrained electrostatic potential (RESP)[49−51] partial charges (Tables S1 and S2, Supporting Information). Geometry optimization and the electrostatic potential calculations were performed at the HF/6-31G* level of the Gaussian09 suite.[52] A nonbonded approach was used for the catalytic zinc atoms. Zinc atom was assigned a formal charge of +2.0 and a van der Waal's radius of 1.10 Å according to previously derived parameters.[53] Finally, each complex was solvated in a rectangular pre-equilibrated box of TIP3P[54] water. Sufficient solvent was added to provide a minimum distance of 10 Å between any protein atom and the edge of the box. This yielded a simulation box containing about 10000 water molecules with initial dimensions of 70 Å × 78 Å × 65 Å.

Molecular Dynamics Simulation. All MD simulations were performed using AMBER10. Initially, energy minimization was carried out for each solvated complex by two steps. In each step, energy minimization was performed by the steepest descent method for the first 3000 steps and conjugated gradient method for the subsequent 2000 steps. During the energy minimization, harmonic restraints with a force constant of 500.0 kcal/(mol·Å^2) was applied to all protein atoms in the first step, and all atoms were allowed to move freely in the second step. After energy minimization, all systems were heated up from 0 to 310.0 K over 100 ps in the *NVT* ensemble and equilibrating to adjust the solvent density under 1 atm pressure over 50 ps in the *NPT* ensemble simulation by restraining all atoms of the structures with a harmonic restraint weight of 10.0 kcal/(mol·Å^2). An additional three MD equilibrations of 50 ps each were performed with the decreased restraint weights of 5.0, 1.0, and 0.1 kcal/(mol·Å^2), respectively. These were followed by a last MD equilibration step of 50 ps by releasing all the restraints. Afterward, production MD simulations were carried out without any restraint on these eight systems in the *NPT* ensemble at a temperature of 310.0 K and a pressure of 1 atm. An integration time step of 2 fs was used, and coordinate trajectory was recorded every 1 ps for all the equilibration and production runs. During the simulations, periodic boundary conditions were employed, and direct space interactions were truncated at a distance 12 Å with long-range contributions from the electrostatics included using the particle mesh Ewald (PME) approach;[55] van der Waals contributions beyond the cutoff were included via the use of an isotropic long-range correction. Bond lengths involving bonds to hydrogen atoms were constrained using the SHAKE algorithm.[56]

Thermodynamic Calculation. The binding free energy of PIs and substrate 4B5A to NS3/4A protease active site was analyzed by the Molecular Mechanics/Generalized Born Surface Area (MM/GBSA) method.[57−60] A single trajectory approach was used with 1000 snapshots at 10 ps interval of each simulation. For each snapshot, we compute the binding free energy (ΔG_{bind}) from

$$\Delta G_{bind} = G_{complex} - G_{receptor} - G_{ligand} \quad (1)$$

$$G_{bind} = E_{gas} + G_{sol} - TS \quad (2)$$

$$E_{gas} = E_{int} + E_{vdW} + E_{ele} \quad (3)$$

$$G_{sol} = G_{GB} + G_{SA} \quad (4)$$

$$G_{SA} = \gamma SASA \quad (5)$$

where E_{gas} is the gas-phase energy; E_{int} is the internal energy; and E_{ele} and E_{vdW} are the Coulomb and van der Waals energies, respectively. E_{gas} was calculated using the ff03 force field. G_{sol} is the solvation free energy and can be decomposed into polar and nonpolar contributions. G_{GB} is the polar solvation contribution calculated by solving the GB equation. G_{SA} is the nonpolar solvation contribution and was estimated by the solvent accessible surface area (SASA) determined using a water probe radius of 1.4 Å. The surface tension constant γ was set to 0.0072 kcal/(mol·Å^2).[61] T and S are the temperature and the total solute entropy, respectively. S was calculated by classical statistical thermodynamics, using normal-mode analysis.[62] Normal mode analysis was carried out in the AMBER10 NMODE module. Due to the high computational cost in the entropy calculation, 100 snapshots were extracted from the last equilibrated 10 ns trajectory of the simulation with 100 ps time intervals, and each snapshot was fully minimized with a distance dependent dielectric function $4R_{ij}$ (the distance between two atoms) until the root-mean-square of the elements of the gradient vector was less than 1×10^{-4} kcal/(mol·Å).

To determine the contribution of individual residue to the total binding free energy between PIs and protease, the MM/GBSA binding free energy decomposition process in AMBER10 was used to decompose the interaction energy to each residue involved in the interaction by considering molecular mechanics and solvation energy without consideration of the contribution of entropy.

Residue Interaction Networks Analysis. The representative structure derived from the last 10 ns trajectory of each system was used for constructing the RIN interactively in 2D graphs. REDUCE[63] was applied for accurately adding hydrogen atoms to 3D protein structure. The eight resulting structural models were used in PROBE,[64] in order to identify noncovalent interaction residues between the atoms of each pair of considered residues. Two residues are defined as in contact if any of their atoms exists in at least one van der Waals interaction.

Interactive Visual Analysis of Residue Networks. The RIN generated from the 3D structures of NS3/4A protease were used to visualize the network by Cytoscape[65] and the plugin RINalyzer.[39] In a RIN, the nodes represent the protein residues and the edges between them represent the noncovalent interactions. The edges are labeled with an interaction type, usually including interatomic contact, hydrogen bond, salt bridge, and so on.

Topological Analysis of Residue Networks. Using the NetworkAnalyzer[66] plugin of Cytoscape, we performed the complex topological parameters analysis of shortest path betweenness and closeness centrality. The betweenness centrality of a node reflects the amount of control that this node exerts over the interactions of other nodes in the network,[67] whereas the closeness centrality is a measure of how quickly information spreads from a given node to other reachable nodes in the network.[68] Both the betweenness and closeness centrality of each node is between 0 and 1.[40]

Comparison of Residue Interaction Networks. In order to highlight and investigate the similarities and differences between the networks corresponding to wild-type and mutant

dx.doi.org/10.1021/ci400060j | J. Chem. Inf. Model. 2014, 54, 621−633

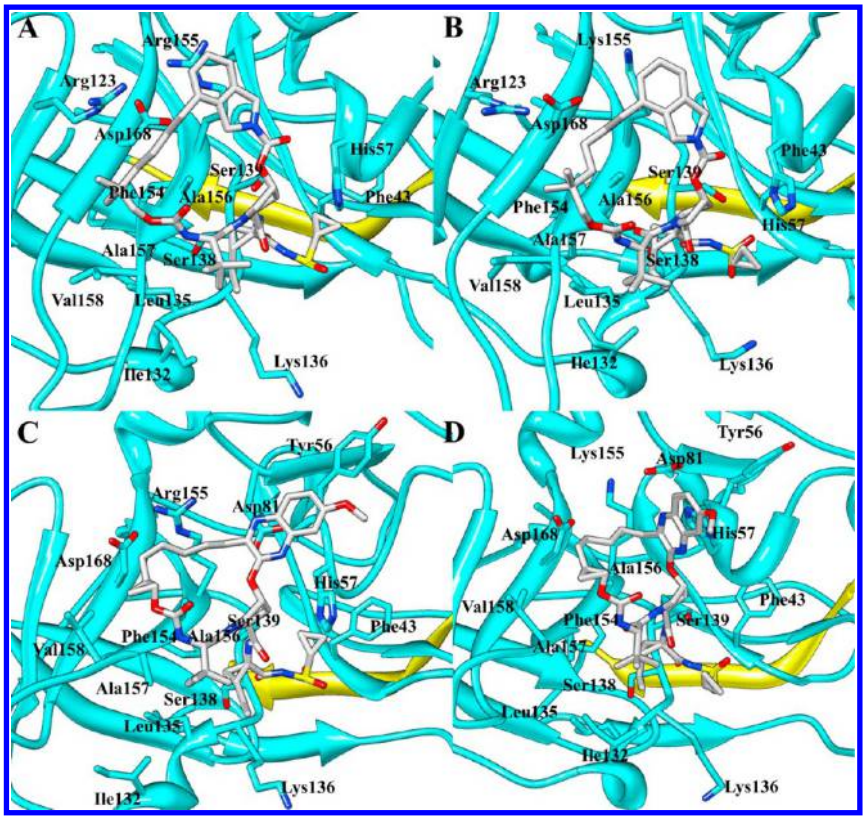

Figure 2. Structural models of (A-B) vaniprevir and (C-D) MK-5172 in a complex with wild-type and R155K mutant NS3/4A protease. The representative structures extracted from the MD trajectories were used. The proteins are shown in cartoon representation with NS3 in cyan and NS4A yellow. The vaniprevir and MK-5172 are shown in a gray stick model.

NS3/4A protease, we generated a combined comparison network of two RIN using RINalyzer based on the superposition alignment of the corresponding 3D structures. The comparison network contains different types of edges and nodes according to the preserved residue interactions and the aligned residues. The type of each node and edge is stored as an attribute, which can be used to visually adjust the network view. Dashed or dotted edges between aligned residue nodes indicate that the corresponding residues form functionally distinct interactions in the two structures.

Substrate Envelope Analysis. The HCV NS3/4A substrate bound to the active site of the protease often with a conserved consensus volume which is defined as the substrate envelope.[46] In addition, HCV NS3/4A PIs also adopt a conserved consensus volume in the binding site of the enzyme. Herein, in order to understand the drug resistance mechanism of known primary mutation sites (R155K, A156T, and D168A) and help design the drug molecule to mimic the exact shape of the substrate of the NS3/4A, the simulated structures of 4B5A were superimposed onto the two simulated drugs binding site of the different simulated systems.

RESULTS AND DISCUSSION

Molecular Dynamics Simulation. The structural dynamics of vaniprevir, MK-5172, and 4B5A bound wild-type protease and R155K, A156T, and D168A mutants were analyzed by performing 30 ns MD simulation. The system stability and overall convergence of simulations was monitored in terms of root-mean-square deviation (RMSD) of protein backbone atoms and active site residues (around 5 Å of ligand) backbone atoms as well as ligand heavy atoms with respect to the initial structure as a function of time. As can be seen from Figures S1 and S2 (Supporting Information), the protein backbone atoms RMSD of vaniprevir, MK-5172, and 4B5A bound wild-type protease and R155K, A156T, and D168A mutant systems in the simulation fluctuates around 2.5, 2.0, 2.8, 2.2, 1.9, 1.8, 1.3, 1.6, 1.3, 1.6, 1.4, and 1.6 Å after 20 ns simulation. According to the active site residues backbone atoms RMSD, there are relatively large fluctuations in vaniprevir bound D168A and MK-5172 bound R155K mutant during the first 20 ns simulation. This is mainly because of the obvious conformation change of the residues His57 and Arg123 in vaniprevir bound D168A mutant and the residues Tyr56, His57, and Asp81 in MK-5172 bound R155K mutant (Figure 2 and Figure S2 (Supporting Information)). However, the fluctuation gradually reaches to about 1.7 Å and 1.3 Å at 20 ns and remains nearly constant in the next 10 ns (Figure S1D and S1F, Supporting Information). Overall, the RMSD fluctuation of all the simulated system with 1.0 Å and the structure for each system remains stable after 20 ns of simulation. Hence, the trajectory of last 10 ns simulation for each system was taken for the following structural and energetic analysis.

Binding Free Energy Calculation. The components of molecular mechanics and solvation energy represent average quantities calculated over the last 10 ns simulation by the MM/GBSA method are listed in Table 1. As shown in Table 1, the predicted binding free energies (ΔG_{bind}) between the protease and inhibitors are correlated well with the experimental IC_{50} values, except for the MK-5172 bound A156T and D168A mutant complexes. In vaniprevir bound complexes, the calculated van der Waals contributions (ΔE_{vdW}) to the binding free energy are different from each other, with values ranging

dx.doi.org/10.1021/ci400060j | J. Chem. Inf. Model. 2014, 54, 621−633

Table 1. Calculated Binding Free Energies Based on the MM/GBSA Method

system		contribution[a]									
		ΔE_{ele}	ΔE_{vdW}	ΔG_{SA}	ΔG_{GB}	ΔE_{gas}[b]	ΔG_{sol}[c]	ΔE_{bind}[d]	$-T\Delta S$	ΔG_{bind}[e]	IC_{50} (nM)[f]
vaniprevir	WT	−33.87 ± 0.18	−69.41 ± 0.10	−7.34 ± 0.01	58.36 ± 0.14	−103.28 ± 0.19	51.02 ± 0.14	−52.26 ± 0.12	28.34 ± 0.38	−23.92	0.34
	R155K	−35.91 ± 0.16	−61.54 ± 0.11	−6.77 ± 0.01	56.35 ± 0.12	−97.45 ± 0.19	49.58 ± 0.12	−47.87 ± 0.12	28.58 ± 0.38	−19.29	>400
	A156T	−35.03 ± 0.19	−59.79 ± 0.11	−6.52 ± 0.01	52.13 ± 0.13	−94.82 ± 0.19	45.61 ± 0.13	−49.21 ± 0.12	27.87 ± 0.53	−21.34	5.7
	D168A	−24.93 ± 0.23	−59.28 ± 0.11	−6.35 ± 0.01	49.94 ± 0.19	−84.21 ± 0.24	43.59 ± 0.19	−40.63 ± 0.11	25.93 ± 0.51	−14.70	>400
MK-5172	WT	−46.47 ± 0.19	−60.17 ± 0.15	−6.49 ± 0.01	63.75 ± 0.16	−106.64 ± 0.24	57.26 ± 0.16	−49.38 ± 0.16	28.01 ± 0.49	−21.37	0.11
	R155K	−45.88 ± 0.18	−53.54 ± 0.12	−5.70 ± 0.02	58.09 ± 0.13	−99.42 ± 0.19	52.39 ± 0.12	−47.03 ± 0.13	26.04 ± 0.57	−20.99	0.55
	A156T	−43.34 ± 0.17	−55.97 ± 0.09	−5.69 ± 0.01	56.23 ± 0.14	−99.30 ± 0.20	50.54 ± 0.13	−48.76 ± 0.12	28.25 ± 0.47	−20.51	108
	D168A	−39.56 ± 0.19	−58.96 ± 0.19	−6.45 ± 0.02	57.07 ± 0.21	−98.52 ± 0.31	50.63 ± 0.19	−47.89 ± 0.16	29.16 ± 0.54	−18.73	13
4B5A	WT	−233.39 ± 1.09	−40.33 ± 0.11	−5.43 ± 0.01	241.89 ± 1.01	−273.72 ± 1.08	236.46 ± 1.01	−37.26 ± 0.16	25.52 ± 0.51	−11.74	
	R155K	−271.78 ± 1.73	−40.33 ± 0.13	−5.99 ± 0.01	278.91 ± 1.63	−312.11 ± 1.73	272.92 ± 1.61	−39.19 ± 0.25	26.56 ± 0.52	−12.63	
	A156T	−222.49 ± 0.92	−40.59 ± 0.12	−5.75 ± 0.01	227.28 ± 0.80	−263.08 ± 0.91	221.53 ± 0.80	−41.55 ± 0.23	27.24 ± 0.45	−14.31	
	D168A	−250.87 ± 1.22	−43.12 ± 0.12	−5.88 ± 0.01	262.43 ± 1.15	−293.99 ± 1.22	256.55 ± 1.14	−37.44 ± 0.17	26.54 ± 0.41	−10.90	

[a] All energies are in kcal/mol, with corresponding standard errors. [b] $\Delta E_{gas} = \Delta E_{int} + \Delta E_{vdW} + \Delta G_{ele}$. [c] $\Delta G_{sol} = \Delta G_{SA} + \Delta G_{GB}$. [d] $\Delta E_{bind} = \Delta E_{gas} + \Delta G_{sol}$. [e] $\Delta G_{bind} = \Delta E_{bind} - T\Delta S$. [f] IC_{50} is derived from the experimental values in the references.[44]

from −69.41 to −59.28 kcal/mol. Compared with vaniprevir bound complexes, ΔE_{vdW} in the MK-5172 bound complex are higher than the former, ranging from −60.17 to −53.54 kcal/mol. In contrast, the calculated electrostatic contributions (ΔE_{ele}) to the binding free energy for MK-5172 bound complexes (ranging from −46.67 to −39.56 kcal/mol) are lower than that for the vaniprevir bound complexes (ranging from −35.91 to −24.93 kcal/mol). The calculated solvation contributions (ΔG_{sol}, $\Delta G_{sol} = \Delta G_{SA} + \Delta G_{GB}$) to the binding free energy for vaniprevir bound complexes (ranging from 43.59 to 51.02 kcal/mol) are lower than that for the MK-5172 bound complexes (ranging from 50.54 to 57.26 kcal/mol). Since MM/GBSA calculations do not include entropic terms, we estimated the corresponding entropic contributions ($-T\Delta S$) upon binding of vaniprevir and MK-5172 for wild-type protease and mutant which were ranging from 25.93 to 29.36 kcal/mol, indicating that conformational change plays an important role to protein−ligand interactions and the incorporation of an entropic term would enable us to predict the final binding free energy (ΔG_{bind}) difference of vaniprevir and MK-5172 to the wild-type protease and mutant more accurately. The free energy components given in Table 1 suggest that the majority of the favorable contributions observed for vaniprevir and MK-5172 binding are ΔE_{vdW} and ΔE_{ele}, whereas the ΔG_{sol} and $-T\Delta S$ have unfavorable contribution to the binding energy. The estimation of the binding free energy of substrate 4B5A binding to the wild-type and mutant NS3/4A protease are also shown in Table 1, which enable us to understand the substrate binding process in detail. The van der Waals interactions energies (ranging from −43.12 to −40.33 kcal/mol) and the nonpolar solvation energies (ranging from −5.99 to −5.43 kcal/mol) responsible for the burial of substrate's hydrophobic groups upon binding are the basis for favorable binding free energies. The favorable Coulomb interactions energies (ranging from −271.78 to −222.49 kcal/mol) are counteracted by the unfavorable polar solvation energies (ranging from 227.28 to 278.91 kcal/mol).

Binding Mode between Vaniprevir and MK-5172 with Wild-Type and Mutant NS3/4A Protease. The representative structures for the eight MD simulations are depicted in Figure 2 and Figure S2 (Supporting Information). The representative structure of each complex is from their conformational ensemble as inferred from the corresponding RMSD using the average structure as a reference of the equilibrated trajectory. The binding modes of vaniprevir and MK-5172 at the wild-type NS3/4A protease active site are shown in Figure 2A and Figure 2C. Vaniprevir and MK-5172 are HCV NS3/4A PIs which contain a P2 to P4 macrocyclic constraint designed using a molecular modeling derived strategy.[14,69] In Figure 2A and Figure 2C, the P2 to P4 linker region of vaniprevir and MK-5172 bind at the S2 and extended S2 subsite and extensively interact with residues Arg155, Ala156, and Asp168. However, the extended P2 isoindoline moiety of vaniprevir extends further into the extended S2 subsite of the active site than MK-5172, suggesting that the former has stronger hydrophobic contacts with the side chain of Arg155 and Ala156 (Figure 2A). This corresponds to the van der Waals energy contributions of the residues Arg155 and Ala156 from the binding free energy decomposition calculation. The van der Waals energies contributions from the residues Arg155 and Ala156 are −3.96 and −3.56 kcal/mol for vaniprevir, whereas the contributions are −2.60 and −2.90 kcal/mol for MK-5172. Instead of the interactions with Arg155

dx.doi.org/10.1021/ci400060j | J. Chem. Inf. Model. 2014, 54, 621−633

and Ala156, the extended P2 quinoxaline moiety of MK-5172 stacks strongly against residues Tyr56, His57, and Asp81 (Figure 2C).

By comparison analysis on the dynamics of the complexes, it can be seen that mutations at position 155, 156, and 168 affect the binding mode of vaniprevir and MK-5172 as well as the conformation of the active site of NS3/4A protease. First, there is a particular difference in orientation of the side chains of residues 155, 156, and 168 in both vanprevir and MK-5172 bound wild-type NS3/4A protease and mutant and residues 56, 57, and 81 in MK-5172 bound protease and mutant (Figure 2 and Figure S2 (Supporting Information)). In order to clearly investigate the conformational rearrangement of vaniprevir and MK-5172 binding site upon mutations, the studied mutant complexes were superposed onto the wild-type (Figure 3 and

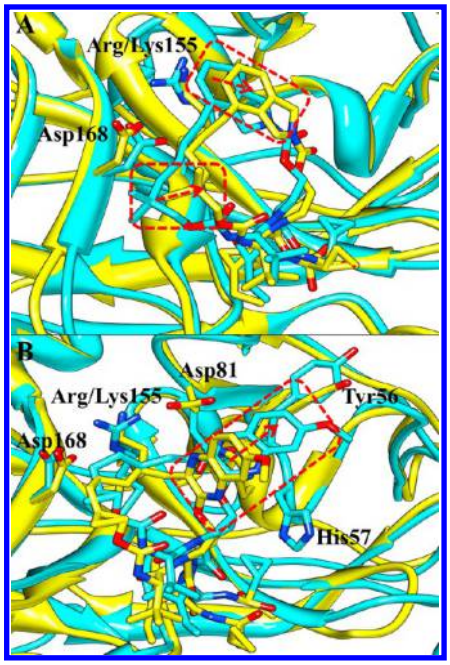

Figure 3. Superimposition of the (A) vaniprevir and (B) MK-5172 bound wild-type and R155K mutant complexes. Cartons of the wild-type (cyan) and the R155K mutant (yellow) are shown. Inhibitors and the selected residues are shown as a stick representation in the wild-type (cyan) and the R155K mutant (yellow) systems.

Figure S4 (Supporting Information)). In addition, the distance between the centroid of selected groups (extended P2 moiety and P2 to P4 linker) of vaniprevir and MK-5172 and the important residues of the wild-type and mutant NS3/4A protease were calculated and listed in Table 2. It is shown in Table 2 that in the mutant complex, the distance between the selected groups of inhibitors and the important residues is increased. Second, it reveals that vaniprevir and MK-5172 have to adopt a compromise position in order to optimize interactions in mutant complexes (Figure 3 and Figure S4 (Supporting Information)). The RMSD values for the heavy atoms of inhibitors are 2.32, 3.05, and 2.38 Å for vaniprevir and 3.42, 2.67, and 2.71 Å for MK-5172 in R155K, A156T, and D168A mutants by using the structure in the wild-type as a reference. Therefore, the mutations change the interaction between vaniprevir and MK-5172 with NS3/4A protease. In the subsequent section, we examined the detailed interaction differences between vanprevir and MK-5172 with wild-type and

Table 2. Calculated the Distance (Å) between the Centroid of Selected Groups (Extended P2 Moiety and P2 to P4 Linker) of Vaniprevir and MK-5172 and the Important Residues of Wild-Type (WT) and Mutant Protease[a]

		systems			
inhibitors	distance	WT	R155K	A156T	D168A
vaniprevir	d1	2.57	5.45		4.66
	d2	5.95		6.94	
	d3	5.98	7.17	7.96	5.02
MK-5172	d4	5.70	9.88	7.06	8.44
	d5	4.90	6.76		6.37
	d6	5.28	8.73	7.68	5.40
	d7	8.75	9.07		
	d8	5.43		6.72	
	d9	5.93		9.29	6.64

[a]d1, the distance between the centroid of extended P2 isoindoline moiety of vaniprevir and the residue 155 of protease. d2 and d3, the distance between the centroid of P2 to P4 linker of vaniprevir and the residue 156 and 168 of protease. d4−d7, the distance between the centroid of extended P2 quinoxaline moiety of MK-5172 and the residues 56, 57, 81, and 155 of protease. d8 and d9, the distance between the centroid of P2 to P4 linker of MK-5172 and the residue 156 and 168 of protease.

mutant NS3/4A protease using free energy change, RIN topological, and substrate envelope analysis.

Molecular Basis of Drug Resistance. *Insight from the Binding Free Energy Calculation.* As shown in Table 1, the predicted binding free energy of vaniprevir and MK-5172 in complex with wild-type and R155K, A156T, and D168A mutant are −23.92, −19.29, −21.34, −14.70, −21.37, −20.99, −20.51, and −18.73 kcal/mol, respectively. Compared with the wild-type complex, the R155K, A156T, and D168A mutant complexes have lower binding free energies. This suggests that vaniprevir and MK-5172 bind less strongly to all three mutants than that of wild-type NS3/4A protease.

The total binding free energy was further decomposed into contributions from each NS3/4A protease residue. Figure 4 and Figures S5 and S6 (Supporting Information) show the comparison of protein−ligand interaction spectra between wild-type with R155K, A156T, and D168A mutant. The energy decomposition analysis shows that, in the vaniprevir bound wild-type NS3/4A protease complex, the main contributions are −3.49, −3.41, −3.11, −2.32, −1.94, −1.30, and −1.21 kcal/mol from residues Ala157, Asp168, Ala156, His57, Arg155, Gly137, and Lys136, respectively. For the MK-5172 bound wild-type NS3/4A protease complex, the main contributions are −3.43, −3.07, −2.87, −1.85, −1.52, −1.33, −1.26, and −0.85 kcal/mol from residues His57, Ala157, Ala156, Lys136, Gly137, Asp168, Tyr56, and Asp81, respectively. In spite of the residue Arg155 showing less contribution (−0.73 kcal/mol) to the interaction energy for the MK-5172 bound wild-type NS3/4A protease complex, there are some contributions from residues Tyr56 (−1.26 kcal/mol) and Asp81 (−0.85 kcal/mol).

For the R155K mutant, the contributions from residues Lys155 and Asp168 are decreased by 3.52 and 1.15 kcal/mol for vaniprevir. Figure 2A indicates that binding of vaniprevir involves an induced-fit mechanism in an extended S2 subsite of wild-type NS3/4A protease, and the residue Arg155 adopts a conformation favorable to interact with the isoindoline of vaniprevir. The R155K mutation results in the isoindoline moiety of vaniprevir to move away and have an unfavorable

dx.doi.org/10.1021/ci400060j | J. Chem. Inf. Model. 2014, 54, 621−633

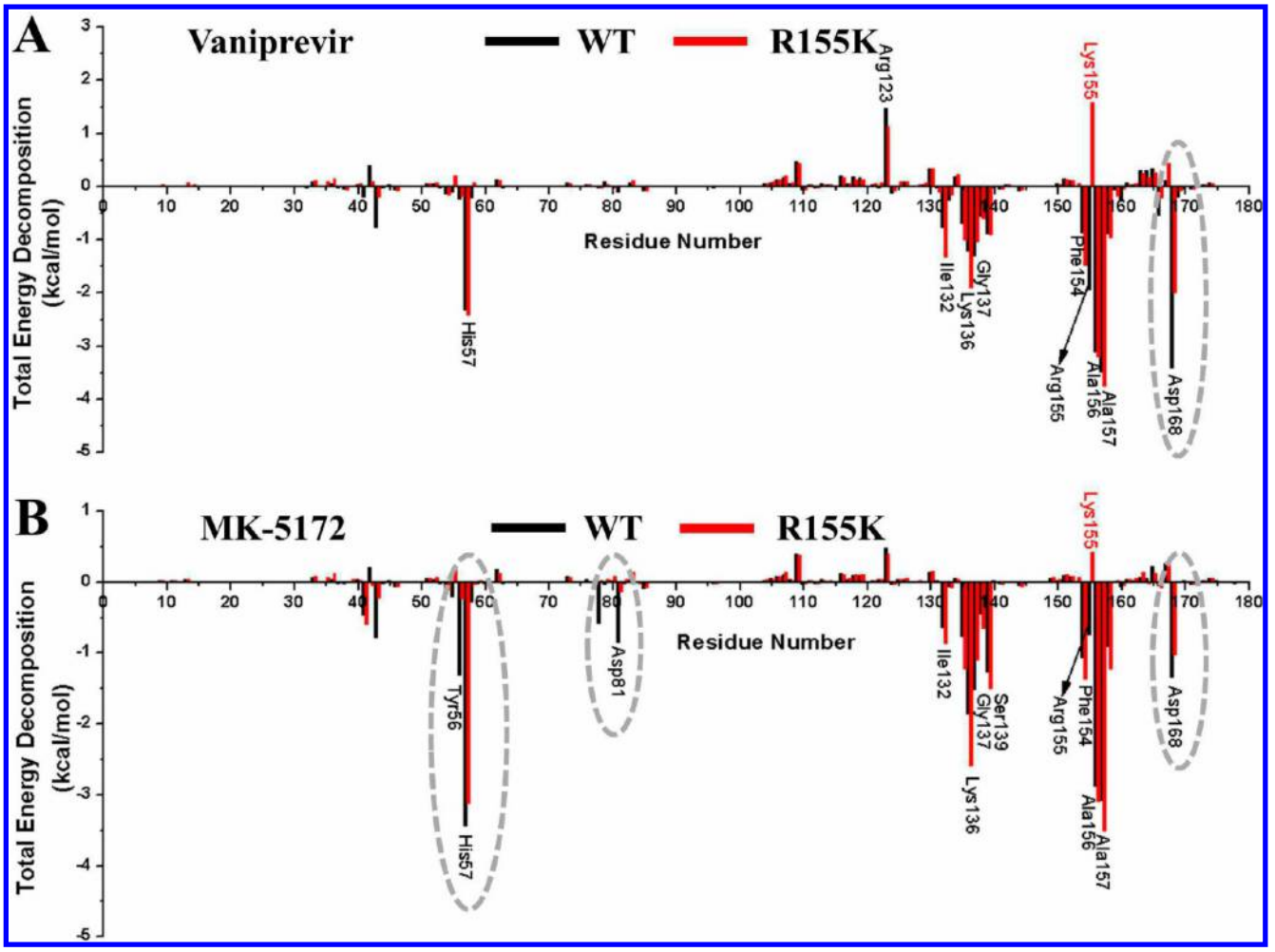

Figure 4. Per-residue interaction spectrum of the residues of NS3/4A with (A) vaniprevir and (B) MK-5172 in complex with wild-type and R155K mutant NS3/4A protease from MM/GBSA free energy decomposition analysis.

contribution to the energy. However, the contributions from residues Tyr56, Asp81, Lys155, and Asp168 are decreased by 1.08, 0.72, 1.40, and 0.31 kcal/mol for MK-5172 bound R155K mutant NS3/4A protease.

As for the A156T mutant, the contributions from Asp168 are decreased by 2.07 kcal/mol for vaniprevir, and contributions from Tyr56, Asp81, Lys136, and Asp168 are decreased by 0.48, 1.06, 0.87, and 0.53 kcal/mol for MK-5172. However, an increase in the contribution is observed from Thr156 with 1.64 and 1.42 kcal/mol for vaniprevir and MK-5172, respectively. The increase in the interaction energy for Thr156 is mainly from the bulky size of the hydrophobic side chain of threonine in the mutant protease. As shown in Table 3, the decomposed van der Waals and electrostatic energies for residue 156 in vaniprevir and MK-5172 bound wild-type and A156T mutant complexes suggest that the increase in the interaction energy is mainly from van der Waals energies contribution. When the aspartate at position 168 is replaced by alanine, the contribution to the free energy from this residue is decreased by 2.31 and 0.72 kcal/mol for vaniprevir and MK-5172, respectively. In addition, this mutant also causes a decrease of the contributions from Tyr56 (1.06 kcal/mol), His57 (1.35 kcal/mol), and Asp81 (0.49 kcal/mol) for MK-5172.

Table 3. Decomposed van der Waals and Electrostatic Energies (kcal/mol) for Residue 156 in Vaniprevir and MK-5172 Bound Wild-Type (WT) and A156T Mutant Complexes

	vaniprevir		MK-5172	
	van der Waals	electrostatic	van der Waals	electrostatic
WT	−3.56	−1.43	−2.90	−1.25
A156T	−4.06	−1.46	−3.64	−1.46

In all vaniprevir bound mutants, the contribution to the free energy from residues 155 and 168 is decreased much more than that in the MK-5172 bound mutant. This is because the large P2 moiety of vaniprevir strongly interacts with Arg155 and Asp168 in the extended S2 subsite (Figure 3A). Thus, mutation at the position of 155 or 168 can directly weaken the interaction between these residues and vaniprevir. For the A156T mutant, the P2 group of vaniprevir is forced to leave the favorable position by the longer side chain attached to the methyl group of Thr156, which further makes the extended P2 moiety and P2 to P4 linker of vaniprevir move away from the extended S2 subsite. This indirectly influenced the interaction between vaniprevir with Arg155 and Asp168. In addition, contributions from residues 56 and 81 for MK-5172 binding are reduced in all mutants.

Insight from the Topological Analysis of the RIN. Network analysis of protein structure has been widely applied to explore the key residues that play the role of "hubs" in the network of

dx.doi.org/10.1021/ci400060j | J. Chem. Inf. Model. 2014, 54, 621−633

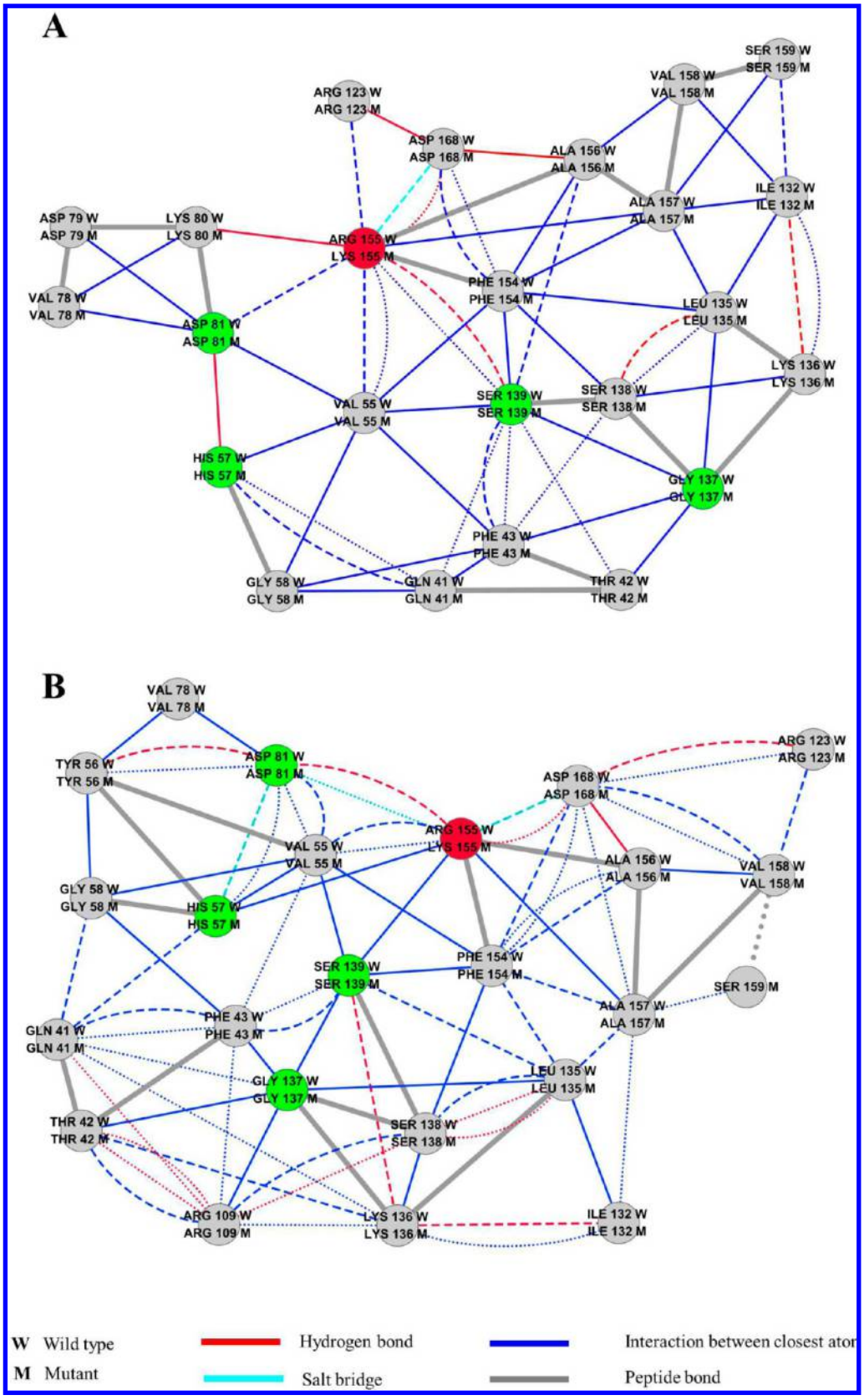

Figure 5. A detailed view of the covalent and noncovalent interactions of the active site nodes (amino acids) in the comparison network of (A) vaniprevir and (B) MK-5172 bound wild-type and R155K mutant NS3/4A protease. Edge line styles correspond to noncovalent residue interactions that are preserved in both complex (solid lines), present only in the wild-type (dashed lines) or only in the R155K mutant (dotted lines). The catalytic residues are colored green and mutated residues red. All other residues are colored gray.

dx.doi.org/10.1021/ci400060j | J. Chem. Inf. Model. 2014, 54, 621−633

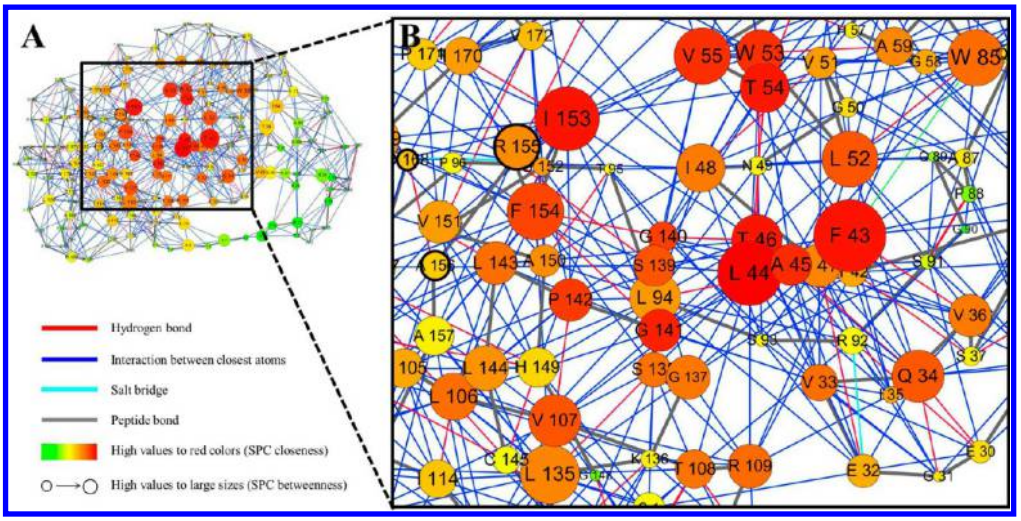

Figure 6. Residue interaction network (RIN) of the vaniprevir bound wild-type NS3/4A protease. Different views of the corresponding RIN are displayed in (A) and (B). The edges are colored with respect to their interaction type. Shortest path betweenness and closeness centrality are denoted by nodes size and color, respectively.

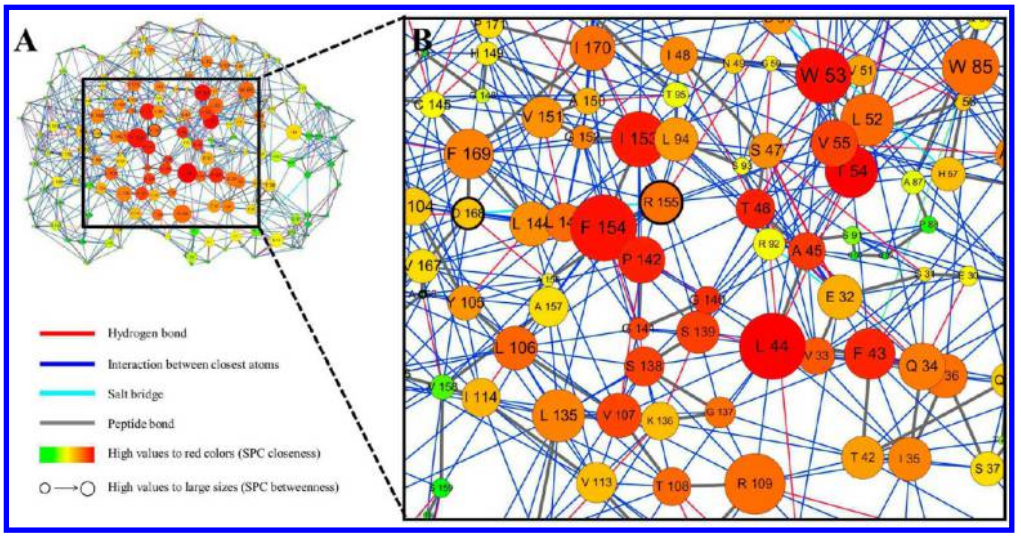

Figure 7. Residue interaction network (RIN) of the MK-5172 bound wild-type NS3/4A protease. Different views of the corresponding RIN are displayed in (A) and (B). The edges are colored with respect to their interaction type. Shortest path betweenness and closeness centrality are denoted by nodes size and color, respectively.

protein folding and allosteric modulation systems.[70] Herein, we investigated the relationship between the small-world network behavior and the drug resistance mutations using the representative protein structures obtained from MD simulation. Figures S7−S12 (Supporting Information) gave an overview of the comparison network of vaniprevir and MK-5172 bound wild-type and R155K, A156T, and D168A mutant NS3/4A protease. The network edge line styles correspond to covalent and noncovalent residue interactions that are preserved in both proteases (solid lines), present only in the wild-type (dashed lines), or only in the R155K, A156T, and D168A mutant (dotted lines) protease. A detailed view of the comparison networks in the catalytic site is shown in Figure 5 and Figure S13 (Supporting Information). It is clear from the comparison networks that the noncovalent residue interactions are different in the wild-type and mutant protease active site. As shown in Figure 5A, there are close atoms interactions between the residues Arg155 and Asp81 and Arg123 in the vaniprevir bound wild-type protease, whereas there are close atoms interactions between the residues Lys155 and Ser139 and hydrogen bond interactions between the residues Lys155 and Asp168 in the R155K mutant protease. For MK-5172 bound protease, the hydrogen bond interactions between the residue Arg155 and Asp81 in the wild-type protease changed to the salt bridge interaction between the residues Lys155 and Asp81 in the mutant protease, and the residue Lys155 formed hydrogen bond interaction with Asp168 (Figure 5B). In the A156T mutant protease, the residue Thr156 formed the close atoms interaction with Asp68 and His57 in both vaniprevir and MK-5172 bound protease, respectively (Figures S13A and S13C, Supporting Information). The hydrogen bond interactions between the residues Asp168 and Arg123 in the wild-type protease changed to the close atoms interactions between the residues Ala168 and Arg123 in both vaniprevir and MK-5172 bound D168A mutant protease (Figure S13B and S13D, Supporting Information). In both the R155K and D168A mutant protease, the salt-bridge interaction between residues 155 and 168 was broken (Figure 5 and Figure S13B and S13D

dx.doi.org/10.1021/ci400060j | J. Chem. Inf. Model. 2014, 54, 621−633

(Supporting Information)). It is reported that the extended S2 subsite is stabilized by this salt bridge,[30,71] thus the interactions between the extended S2 subsite (especially for residues 155 and 168) with the P2 moiety and P2 to P4 linker region of vaniprevir and MK-5172 was influenced in the R155K and D168A mutant complexes.

In addition, network analysis of protein structures has shown that amino acid with high shortest path betweenness values involved in stabilizing the protein structures and the residues with high closeness values are likely to be functionally important.[72−74] Therefore, we further computed the shortest path betweenness and closeness centrality of each node (amino acid) in the network of vaniprevir and MK-5172 bound wild-type and R155K, A156T, and D168A mutant NS3/4A protease (Tables S3 and S4, Supporting Information). We compared the shortest path centrality of the network analysis for RIN and enables dynamic 2D views in Figure 6, Figure 7, and Figures S14−S19 (Supporting Information), with the shortest path betweenness and closeness centrality denoted by node size and color. As shown in Figure 6, Figure 7, and Figures S14−S19 (Supporting Information), it is highlighted that residues with a high betweenness and closeness value in the network are located at the active site of the protease. However, we found that the three main drug resistance mutations (residue 155, 156, and 168) occur at protease residues often with a relatively low betweenness and closeness value.

Insight from the Substrate Envelope Analysis. Several reported studies have shown that substrate envelope hypothesis is very useful in explaining the molecular mechanism of the natural substrate recognition to HCV NS3/4A protease as well as the resistance mechanism to PIs.[30,44,75,76] Herein, the substrate 4B5A extracted from the wild-type and mutant complex were superposed onto the active site of NS3/4A protease and shown in Figure 8. The substrate 4B5A in

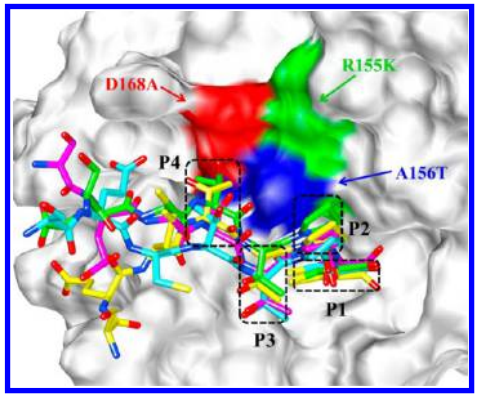

Figure 8. Superimposition of the substrate extracted from wild-type and mutant NS3/4A protease complexes. 4B5A are represented as a stick model and colored green, yellow, cyan, and pink in wild-type, R155K, A156T, and D168A mutant NS3/4A protease complexes, respectively. Peptide sites P1, P2, P3, and P4 directly transferred to inhibitors are indicated.

different systems adopts a conserved consensus volume in the peptide sites P1, P2, P3, and P4, and this conserved consensus volume has less contacts with the three drug resistance mutation sites. The substrate 4B5A was further superposed onto the active site of vaniprevir and MK-5172 bound wild-type and R155K, A156T and D168A mutant NS3/4A protease (Figure 9 and Figure S20 (Supporting Information)). Three main drug resistance mutations at residues 155, 156, and 168

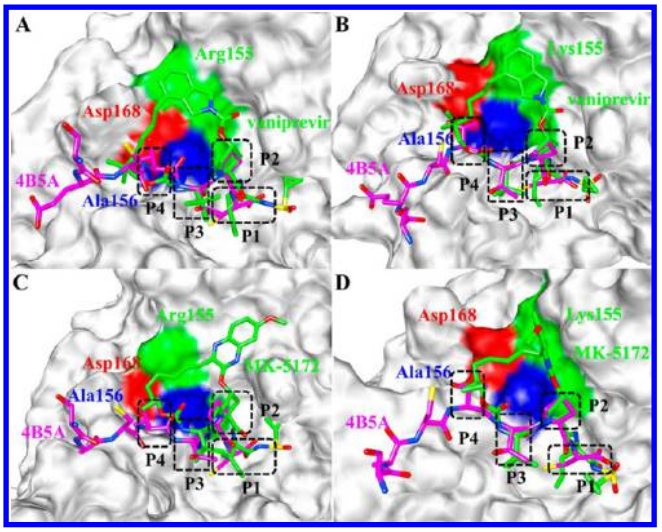

Figure 9. Molecular surface representation of the active site structure of the (A-B) vaniprevir and (C-D) MK-5172 bound wild-type and R155K mutant NS3/4A protease complexes as well as the superimposed 4B5A substrate from the MD simulation. The mutated NS3/4A protease residues which confer drug resistance are particularly labeled. Inhibitors (green) and substrate (pink) are represented as a stick model. Peptide sites P1, P2, P3, and P4 directly transferred to inhibitors are indicated.

have good contact with the P2 to P4 linker region where vaniprevir and MK-5172 volume deviates from the substrate envelope. In contrast, our previous work demonstrated that these residues had little contribution to the binding of substrate 4B5A.[77] Additionally, the molecular surface in Figure 9 and Figure S20 (Supporting Information) demonstrates that in R155K, A156T, and D168A mutant NS3/4A protease, the binding of vaniprevir and MK-5172 are protruded from the substrate envelope and there is a conformational rearrangement at the active site. This rearrangement is likely to limit the capacity of the active site to accommodate vaniprevir and MK-5172. Therefore, the drug resistance mutation of the residue outside of the substrate envelope may selectively decrease the affinity of inhibitor but not the activity of the enzyme and consequently help NS3/4A protease escape from the inhibition without influencing substrate binding.

As mentioned above, the extended P2 isoindoline moiety of vaniprevir interacting extensively at the extended S2 subsite and the R155K and D168A mutation disrupted the favorable interactions with the extended P2 moiety, causing significant drug resistance. However, MK-5172 adopted a novel conformation with the extended P2 quinoxaline moiety not interacting extensively with R155 and D168 but contacting with Tyr56, His57, and Asp81. The energy loss of these residues can explain why these mutations have less effect on the binding of MK-5172. In addition, P2 of vaniprevir and MK-5172 has van der Waals interactions Ala156 in wild-type. The A156T mutant forces the P2 of vaniprevir and MK-5172 to move away due to the steric clash and further leads to a decrease of the drugs affinity. Therefore, based on the comparison in structural and energetic features of vaniprevir and MK-5172 binding to the wild-type and mutant NS3/4A protease as well as the substrate envelope analysis, we suggest the following strategies for the future structure based drug design of inhibitors against resistance. First, inhibitors should not contain to a large extent P2 moiety and optimizing the macrocycle makes less contact

dx.doi.org/10.1021/ci400060j | J. Chem. Inf. Model. 2014, 54, 621−633

with Ala156. A recent study has shown that the installation of a fused ring linker can lead to improvement in the activity targeting A156T mutant. The molecular modeling results also suggest that the fused cyclopropyl constraint of the inhibitor seems to shift the macrocycle away from the A156 residue.[14] Second, the P2 moiety and P2 to P4 linker for the inhibitors should be optimized. The P2 to P4 linker of the inhibitors protrudes the substrate envelope and has contact with known primary drug resistance mutation sites (Arg155, Ala156, and Asp168). Therefore, designing compounds that mimic the shape of the product peptide substrate of NS3/4A protease, especially the peptide sites P1, P2, P3, and P4, may decrease the probability of drug resistance.

CONCLUSIONS

In this study, we investigated the structural and energetic features of wild-type HCV NS3/4A protease and its three drug resistant variants to vaniprevir and MK-5172 through the combination use of MD simulation, binding free energy calculation, free energy decomposition, RIN, and substrate envelope analysis. MD simulation results revealed the structural basis of drug resistance conferred by these mutations. Detailed binding free energy calculation demonstrates that the studied mutations alter the binding motif of vaniprevir and MK-5172 and weaken the protein−ligand interactions. Topological analysis of RIN indicates that the three main drug resistance mutation residues of NS3/4A protease have a relatively low betweenness and closeness value in the network. The superimposition of the substrate 4B5A onto the protease active site show that the studied mutations occur at the residues outside the substrate envelope of NS3/4A protease. Therefore, the substitutions of these residues in the mutant selectively weaken inhibitor binding but not the activity of the enzyme and consequently help NS3/4A protease escape from the effect of the inhibitors without influencing the affinity of substrate binding. Our study provides a molecular level explanation for HCV NS3/4A protease drug resistance reported in experimental studies, and the results will be useful for the design and development of new generation NS3/4A PIs with improved potency for the treatment of HCV chronic infection.

ASSOCIATED CONTENT

Supporting Information

Table S1 and S2: The atom types and partial charges for vaniprevir and MK-5172. Tables S3 and S4: Summary of the shortest path betweenness and closeness centrality of each node in the network of vaniprevir and MK-5172 bound complexes. Figure S1 and S2: RMSD of the simulated systems. Figure S3: Structural models of vaniprevir and MK-5172 bound A156T and D168A mutant complexes. Figure S4: Superimposition of the vaniprevir and MK-5172 bound wild-type and mutant (A156T and D168A) complexes. Figures S5 and S6: Per-residue interaction spectrum of the residues of vaniprevir and MK-5172 bound A156T and D168A mutant NS3/4A protease. Figures S7−S12: Comparison network of vaniprevir and MK-5172 bound wild-type and mutant NS3/4A protease. Figure S13: Detailed view of the noncovalent interactions of the active site nodes in the comparison network of vaniprevir and MK-5172 bound A156T and D168A mutant NS3/4A protease. Figures S14−S19: RIN of vaniprevir and MK-5172 bound mutant NS3/4A protease. Figure S20: Substrate envelope analysis of the vaniprevir and MK-5172 bound A156T and D168A mutant complexes. This material is available free of charge via the Internet at http://pubs.acs.org.

AUTHOR INFORMATION

Corresponding Author

*Phone: +86-931-891-2578. Fax: +86-931-891-2582. E-mail: xjyao@lzu.edu.cn.

Notes

The authors declare no competing financial interest.

ACKNOWLEDGMENTS

This work was supported by the National Natural Science Foundation of China (Grant No.21175063) and the Program for Changjiang Scholars and Innovative Research Team in University (Grant No. PCSIRT: IRT1137).

REFERENCES

(1) Melnikova, I. Hepatitis C — Pipeline Update. *Nat. Rev. Drug Discovery* **2011**, *10*, 93−94.

(2) Fried, M. W.; Shiffman, M. L.; Reddy, K. R.; Smith, C.; Marinos, G.; Gonçales, F. L.; Häussinger, D.; Diago, M.; Carosi, G.; Dhumeaux, D.; Craxi, A.; Lin, A.; Hoffman, J.; Yu, J. Peginterferon Alfa-2a plus Ribavirin for Chronic Hepatitis C Virus Infection. *N. Engl. J. Med.* **2002**, *347*, 975−982.

(3) Hadziyannis, S. J.; Sette, H.; Morgan, T. R.; Balan, V.; Diago, M.; Marcellin, P.; Ramadori, G.; Bodenheimer, H.; Bernstein, D.; Rizzetto, M.; Zeuzem, S.; Pockros, P. J.; Lin, A.; Ackrill, A. M. Peginterferon-α2a and Ribavirin Combination Therapy in Chronic Hepatitis C. *Ann. Intern. Med.* **2004**, *140*, 346−355.

(4) Munir, S.; Saleem, S.; Idrees, M.; Tariq, A.; Butt, S.; Rauff, B.; Hussain, A.; Badar, S.; Naudhani, M.; Fatima, Z.; Ali, M.; Ali, L.; Akram, M.; Aftab, M.; Khubaib, B.; Awan, Z. Hepatitis C Treatment: Current and Future Perspectives. *Virol. J.* **2010**, *7*, 296−301.

(5) Feld, J. J.; Hoofnagle, J. H. Mechanism of Action of Interferon and Ribavirin in Treatment of Hepatitis C. *Nature* **2005**, *436*, 967−972.

(6) Klibanov, O. M.; Vickery, S. B.; Olin, J. L.; Smith, L. S.; Williams, S. H. Oceprevir: A Novel NS3/4 Protease Inhibitor for the Treatment of Hepatitis C. *Pharmacotherapy* **2012**, *32*, 173−190.

(7) Matthews, S. J.; Lancaster, J. W. Telaprevir: A Hepatitis C NS3/4A Protease Inhibitor. *Clin. Ther.* **2012**, *34*, 1857−1882.

(8) Ghany, M. G.; Nelson, D. R.; Strader, D. B.; Thomas, D. L.; Seeff, L. B. An Update on Treatment of Genotype 1 Chronic Hepatitis C Virus Infection: 2011 Practice Guideline by the American Association for the Study of Liver Diseases. *Hepatology* **2011**, *54*, 1433−1444.

(9) Bartenschlager, R. The NS3/4A Proteinase of the Hepatitis C Virus: Unravelling Structure and Function of an Unusual Enzyme and a Prime Target for Antiviral Therapy. *J. Viral. Hepat.* **1999**, *6*, 165−181.

(10) Kolykhalov, A. A.; Mihalik, K.; Feinstone, S. M.; Rice, C. M. Hepatitis C Virus-Encoded Enzymatic Activities and Conserved RNA Elements in the 3′ Nontranslated Region Are Essential for Virus Replication In Vivo. *J. Virol.* **2000**, *74*, 2046−2051.

(11) Lin, T. I.; Lenz, O.; Fanning, G.; Verbinnen, T.; Delouvroy, F.; Scholliers, A.; Vermeiren, K.; Rosenquist, A.; Edlund, M.; Samuelsson, B.; Vrang, L.; de Kock, H.; Wigerinck, P.; Raboisson, P.; Simmen, K. In Vitro Activity and Preclinical Profile of TMC435350, a Potent Hepatitis C Virus Protease Inhibitor. *Antimicrob. Agents Chemother.* **2009**, *53*, 1377−1385.

(12) Seiwert, S. D.; Andrews, S. W.; Jiang, Y.; Serebryany, V.; Tan, H.; Kossen, K.; Rajagopalan, P. T. R.; Misialek, S.; Stevens, S. K.; Stoycheva, A.; Hong, J.; Lim, S. R.; Qin, X.; Rieger, R.; Condroski, K. R.; Zhang, H.; Do, M. G.; Lemieux, C.; Hingorani, G. P.; Hartley, D. P.; Josey, J. A.; Pan, L.; Beigelman, L.; Blatt, L. M. Preclinical Characteristics of the Hepatitis C Virus NS3/4A Protease Inhibitor ITMN-191 (R7227). *Antimicrob. Agents Chemother.* **2008**, *52*, 4432−4441.

(13) Liverton, N. J.; Carroll, S. S.; DiMuzio, J.; Fandozzi, C.; Graham, D. J.; Hazuda, D.; Holloway, M. K.; Ludmerer, S. W.; McCauley, J. A.; McIntyre, C. J.; Olsen, D. B.; Rudd, M. T.; Stahlhut, M.; Vacca, J. P. MK-7009, a Potent and Selective Inhibitor of Hepatitis C Virus NS3/4A Protease. *Antimicrob. Agents Chemother.* **2010**, *54*, 305−311.
(14) Harper, S.; McCauley, J. A.; Rudd, M. T.; Ferrara, M.; DiFilippo, M.; Crescenzi, B.; Koch, U.; Petrocchi, A.; Holloway, M. K.; Butcher, J. W.; Romano, J. J.; Bush, K. J.; Gilbert, K. F.; McIntyre, C. J.; Nguyen, K. T.; Nizi, E.; Carroll, S. S.; Ludmerer, S. W.; Burlein, C.; DiMuzio, J. M.; Graham, D. J.; McHale, C. M.; Stahlhut, M. W.; Olsen, D. B.; Monteagudo, E.; Cianetti, S.; Giuliano, C.; Pucci, V.; Trainor, N.; Fandozzi, C. M.; Rowley, M.; Coleman, P. J.; Vacca, J. P.; Summa, V.; Liverton, N. J. Discovery of MK-5172, a Macrocyclic Hepatitis C Virus NS3/4a Protease Inhibitor. *ACS Med. Chem. Lett.* **2012**, *3*, 332−336.
(15) Halfon, P.; Locarnini, S. Hepatitis C Virus Resistance to Protease Inhibitors. *J. Hepatol.* **2011**, *55*, 192−206.
(16) Thompson, A. J.; Locarnini, S. A.; Beard, M. R. Resistance to anti-HCV Protease Inhibitors. *Curr. Opin. Virol.* **2011**, *1*, 599−606.
(17) Rizzo, R. C.; Toba, S.; Kuntz, I. D. A Molecular Basis for the Selectivity of Thiadiazole Urea Inhibitors with Stromelysin-1 and Gelatinase-A from Generalized Born Molecular Dynamics Simulations. *J. Med. Chem.* **2004**, *47*, 3065−3074.
(18) Zhou, Z.; Madrid, M.; Evanseck, J. D.; Madura, J. D. Effect of a Bound Non-Nucleoside RT Inhibitor on the Dynamics of Wild-Type and Mutant HIV-1 Reverse Transcriptase. *J. Am. Chem. Soc.* **2005**, *127*, 17253−17260.
(19) Guo, Z.; Prongay, A.; Tong, X.; Fischmann, T.; Bogen, S.; Velazquez, F.; Venkatraman, S.; Njoroge, F. G.; Madison, V. Computational Study of the Effects of Mutations A156T, D168V, and D168Q on the Binding of HCV Protease Inhibitors. *J. Chem. Theory. Comput.* **2006**, *2*, 1657−1663.
(20) Aruksakunwong, O.; Wolschann, P.; Hannongbua, S.; Sompornpisut, P. Molecular Dynamic and Free Energy Studies of Primary Resistance Mutations in HIV-1 Protease-Ritonavir Complexes. *J. Chem. Inf. Model.* **2006**, *46*, 2085−2092.
(21) Hou, T.; Yu, R. Molecular Dynamics and Free Energy Studies on the Wild-type and Double Mutant HIV-1 Protease Complexed with Amprenavir and Two Amprenavir-Related Inhibitors: Mechanism for Binding and Drug Resistance. *J. Med. Chem.* **2007**, *50*, 1177−1188.
(22) Stoica, I.; Sadiq, S. K.; Coveney, P. V. Rapid and Accurate Prediction of Binding Free Energies for Saquinavir-Bound HIV-1 Proteases. *J. Am. Chem. Soc.* **2008**, *130*, 2639−2648.
(23) Chachra, R.; Rizzo, R. C. Origins of Resistance Conferred by the R292K Neuraminidase Mutation via Molecular Dynamics and Free Energy Calculations. *J. Chem. Theory Comput.* **2008**, *4*, 1526−1540.
(24) Alcaro, S.; Artese, A.; Ceccherini-Silberstein, F.; Ortuso, F.; Perno, C. F.; Sing, T.; Svicher, V. Molecular Dynamics and Free Energy Studies on the Wild-Type and Mutated HIV-1 Protease Complexed with Four Approved Drugs: Mechanism of Binding and Drug Resistance. *J. Chem. Inf. Model.* **2009**, *49*, 1751−1761.
(25) Balius, T. E.; Rizzo, R. C. Quantitative Prediction of Fold Resistance for Inhibitors of EGFR. *Biochemistry* **2009**, *48*, 8435−8448.
(26) Zhang, J.; Hou, T.; Wang, W.; Liu, J. S. Detecting and Understanding Combinatorial Mutation Patterns Responsible for HIV Drug Resistance. *Proc. Natl. Acad. Sci.* **2010**, *107*, 1321−1326.
(27) Cai, Y.; Schiffer, C. A. Decomposing the Energetic Impact of Drug Resistant Mutations in HIV-1 Protease on Binding DRV. *J. Chem. Theory Comput.* **2010**, *6*, 1358−1368.
(28) Liu, H.; Yao, X.; Wang, C.; Han, J. In Silico Identification of the Potential Drug Resistance Sites over 2009 Influenza A (H1N1) Virus Neuraminidase. *Mol. Pharmaceutics* **2010**, *7*, 894−904.
(29) Pan, D.; Sun, H.; Bai, C.; Shen, Y.; Jin, N.; Liu, H.; Yao, X. Prediction of Zanamivir Efficiency over the Possible 2009 Influenza A (H1N1) Mutant by Multiple Molecular Dynamics Simulations and Free Energy Calculations. *J. Mol. Model.* **2011**, *17*, 2465−2473.
(30) Xue, W.; Pan, D.; Yang, Y.; Liu, H.; Yao, X. Molecular Modeling Study on the Resistance Mechanism of HCV NS3/4A Serine Protease Mutant R155K, A156V and D168A to TMC435. *Antiviral Res.* **2012**, *93*, 126−137.
(31) Xue, W.; Qi, J.; Yang, Y.; Jin, X.; Liu, H.; Yao, X. Understanding the Effect of Drug-Resistant Mutations of HIV-1 Intasome on Raltegravir Action through Molecular Modeling Study. *Mol. Biosyst.* **2012**, *8*, 2135−2144.
(32) Pan, D.; Xue, W.; Zhang, W.; Liu, H.; Yao, X. Understanding the Drug Resistance Mechanism of Hepatitis C Virus NS3/4A to ITMN-191 Due to R155K, A156V, D168A/E Mutations: A Computational Study. *Biochim. Biophys. Acta* **2012**, *1820*, 1526−1534.
(33) Li, L.; Li, Y.; Zhang, L.; Hou, T. Theoretical Studies on the Susceptibility of Oseltamivir against Variants of 2009 A/H1N1 Influenza Neuraminidase. *J. Chem. Inf. Model.* **2012**, *52*, 2715−2729.
(34) Vergara-Jaque, A.; Poblete, H.; Lee, E. H.; Schulten, K.; González-Nilo, F.; Chipot, C. Molecular Basis of Drug Resistance in A/H1N1 Virus. *J. Chem. Inf. Model.* **2012**, *52*, 2650−2656.
(35) del Sol, A.; Fujihashi, H.; Amoros, D.; Nussinov, R. Residues Crucial for Maintaining Short Paths in Network Communication Mediate Signaling in Proteins. *Mol. Syst. Biol.* **2006**, *2*, 2006.0019.
(36) Welsch, C.; Schweizer, S.; Shimakami, T.; Domingues, F. S.; Kim, S.; Lemon, S. M.; Antes, I. Ketoamide Resistance and Hepatitis C Virus Fitness in Val55 Variants of the NS3 Serine Protease. *Antimicrob. Agents Chemother.* **2012**, *56*, 1907−1915.
(37) Welsch, C.; Domingues, F.; Susser, S.; Antes, I.; Hartmann, C.; Mayr, G.; Schlicker, A.; Sarrazin, C.; Albrecht, M.; Zeuzem, S.; Lengauer, T. Molecular Basis of Telaprevir Resistance Due to V36 and T54 Mutations in the NS3−4A Protease of the Hepatitis C Virus. *Genome Biol.* **2008**, *9*, R16.
(38) Xue, W.; Jin, X.; Ning, L.; Wang, M.; Liu, H.; Yao, X. Exploring the Molecular Mechanism of Cross-Resistance to HIV-1 Integrase Strand Transfer Inhibitors by Molecular Dynamics Simulation and Residue Interaction Network Analysis. *J. Chem. Inf. Model.* **2012**, *53*, 210−222.
(39) Doncheva, N. T.; Klein, K.; Domingues, F. S.; Albrecht, M. Analyzing and Visualizing Residue Networks of Protein Structures. *Trends Biochem. Sci.* **2011**, *36*, 179−182.
(40) Doncheva, N. T.; Assenov, Y.; Domingues, F. S.; Albrecht, M. Topological Analysis and Interactive Visualization of Biological Networks and Protein Structures. *Nat. Protoc.* **2012**, *7*, 670−685.
(41) Altman, M. D.; Ali, A.; Kumar Reddy, G. S. K.; Nalam, M. N. L.; Anjum, S. G.; Cao, H.; Chellappan, S.; Kairys, V.; Fernandes, M. X.; Gilson, M. K.; Schiffer, C. A.; Rana, T. M.; Tidor, B. HIV-1 Protease Inhibitors from Inverse Design in the Substrate Envelope Exhibit Subnanomolar Binding to Drug-Resistant Variants. *J. Am. Chem. Soc.* **2008**, *130*, 6099−6113.
(42) Nalam, M. N. L.; Ali, A.; Altman, M. D.; Reddy, G. S. K. K.; Chellappan, S.; Kairys, V.; Özen, A.; Cao, H.; Gilson, M. K.; Tidor, B.; Rana, T. M.; Schiffer, C. A. Evaluating the Substrate-Envelope Hypothesis: Structural Analysis of Novel HIV-1 Protease Inhibitors Designed To Be Robust against Drug Resistance. *J. Virol.* **2010**, *84*, 5368−5378.
(43) Parai, M. K.; Huggins, D. J.; Cao, H.; Nalam, M. N. L.; Ali, A.; Schiffer, C. A.; Tidor, B.; Rana, T. M. Design, Synthesis, and Biological and Structural Evaluations of Novel HIV-1 Protease Inhibitors To Combat Drug Resistance. *J. Med. Chem.* **2012**, *55*, 6328−6341.
(44) Romano, K. P.; Ali, A.; Aydin, C.; Soumana, D.; Özen, A.; Deveau, L. M.; Silver, C.; Cao, H.; Newton, A.; Petropoulos, C. J.; Huang, W.; Schiffer, C. A. The Molecular Basis of Drug Resistance against Hepatitis C Virus NS3/4A Protease Inhibitors. *PLoS Pathog.* **2012**, *8*, e1002832.
(45) *The PyMOL Molecular Graphics System*, Version 0.99rc6; DeLano Scientific LLC: Palo Alto, CA, 2008.
(46) Romano, K. P.; Ali, A.; Royer, W. E.; Schiffer, C. A. Drug Resistance against HCV NS3/4A Inhibitors Is Defined by the Balance of Substrate Recognition versus Inhibitor Binding. *Proc. Natl. Acad. Sci.* **2010**, *107*, 20986−20991.
(47) Case, D. A.; Darden, T. A.; Cheatham, T. E., III; Simmerling, C. L.; Wang, J.; Duke, R. E.; Luo, R.; Crowley, M.; Walker, R. C.; Zhang, W.; Merz, K. M.; Wang, B.; Hayik, S.; Roitberg, A.; Seabra, G.; Kolossváry, I.; Wong, K. F.; Paesani, F.; Vanicek, J.; Wu, X.; Brozell, S. R.; Steinbrecher, T.; Gohlke, H.; Yang, L.; Tan, C.; Mongan, J.;

Hornak, V.; Cui, G.; Mathews, D. H.; Seetin, M. G.; Sagui, C.; Babin, V.; Kollman, P. A. *AMBER 10*; University of California: San Francisco, 2008.
(48) Duan, Y.; Wu, C.; Chowdhury, S.; Lee, M. C.; Xiong, G.; Zhang, W.; Yang, R.; Cieplak, P.; Luo, R.; Lee, T.; Caldwell, J.; Wang, J.; Kollman, P. A Point-Charge Force Field for Molecular Mechanics Simulations of Proteins Based on Condensed-Phase Quantum Mechanical Calculations. *J. Comput. Chem.* **2003**, *24*, 1999−2012.
(49) Bayly, C. I.; Cieplak, P.; Cornell, W.; Kollman, P. A. A Well-Behaved Electrostatic Potential Based Method Using Charge Restraints for Deriving Atomic Charges: The RESP Model. *J. Phys. Chem.* **1993**, *97*, 10269−10280.
(50) Cieplak, P.; Cornell, W. D.; Bayly, C.; Kollman, P. A. Application of the Multimolecule and Multiconformational RESP Methodology to Biopolymers: Charge Derivation for DNA, RNA, and Proteins. *J. Comput. Chem.* **1995**, *16*, 1357−1377.
(51) Fox, T.; Kollman, P. A. Application of the RESP Methodology in the Parametrization of Organic Solvents. *J. Phys. Chem. B* **1998**, *102*, 8070−8079.
(52) Frisch, M. J.; Trucks, G. W.; Schlegel, H. B.; Scuseria, G. E.; Robb, M. A.; Cheeseman, J. R.; Scalmani, G.; Barone, V.; Mennucci, B.; Petersson, G. A.; Nakatsuji, H.; Caricato, M.; Li, X.; Hratchian, H. P.; Izmaylov, A. F.; Bloino, J.; Zheng, G.; Sonnenberg, J. L.; Hada, M.; Ehara, M.; Toyota, K.; Fukuda, R.; Hasegawa, J.; Ishida, M.; Nakajima, T.; Honda, Y.; Kitao, O.; Nakai, H.; Vreven, T.; Montgomery, J. A., Jr.; Peralta, J. E.; Ogliaro, F.; Bearpark, M.; Heyd, J. J.; Brothers, E.; Kudin, K. N.; Staroverov, V. N.; Kobayashi, R.; Normand, J.; Raghavachari, K.; Rendell, A.; Burant, J. C.; Iyengar, S. S.; Tomasi, J.; Cossi, M.; Rega, N.; Millam, N. J.; Klene, M.; Knox, J. E.; Cross, J. B.; Bakken, V.; Adamo, C.; Jaramillo, J.; Gomperts, R.; Stratmann, R. E.; Yazyev, O.; Austin, A. J.; Cammi, R.; Pomelli, C.; Ochterski, J. W.; Martin, R. L.; Morokuma, K.; Zakrzewski, V. G.; Voth, G. A.; Salvador, P.; Dannenberg, J. J.; Dapprich, S.; Daniels, A. D.; Farkas, Ö.; Foresman, J. B.; Ortiz, J. V.; Cioslowski, J.; Fox, D. J. *Gaussian 09*; Gaussian, Inc.: Wallingford, CT, 2009.
(53) Stote, R. H.; Karplus, M. Zinc Binding in Proteins and Solution: A Simple but Accurate Nonbonded Representation. *Proteins: Struct., Funct., Bioinf.* **1995**, *23*, 12−31.
(54) Jorgensen, W. L.; Chandrasekhar, J.; Madura, J. D.; Impey, R. W.; Klein, M. L. Comparison of Simple Potential Functions for Simulating Liquid Water. *J. Chem. Phys.* **1983**, *79*, 926−935.
(55) Darden, T.; York, D.; Pedersen, L. Particle Mesh Ewald: An N·log(N) Method for Ewald Sums in Large Systems. *J. Chem. Phys.* **1993**, *98*, 10089−10092.
(56) Ryckaert, J.-P.; Ciccotti, G.; Berendsen, H. J. C. Numerical Integration of the Cartesian Equations of Motion of a System with Constraints: Molecular Dynamics of n-Alkanes. *J. Comput. Phys.* **1977**, *23*, 327−341.
(57) Kollman, P. A.; Massova, I.; Reyes, C.; Kuhn, B.; Huo, S.; Chong, L.; Lee, M.; Lee, T.; Duan, Y.; Wang, W.; Donini, O.; Cieplak, P.; Srinivasan, J.; Case, D. A.; Cheatham, T. E. Calculating Structures and Free Energies of Complex Molecules: Combining Molecular Mechanics and Continuum Models. *Acc. Chem. Res.* **2000**, *33*, 889−897.
(58) Massova, I.; Kollman, P. Combined Molecular Mechanical and Continuum Solvent Approach (MM-PBSA/GBSA) To Predict Ligand Binding. *Perspect. Drug Discovery* **2000**, *18*, 113−135.
(59) Tsui, V.; Case, D. A. Theory and Applications of the Generalized Born Solvation Model in Macromolecular Simulations. *Biopolymers* **2000**, *56*, 275−291.
(60) Onufriev, A.; Bashford, D.; Case, D. A. Modification of the Generalized Born Model Suitable for Macromolecules. *J. Phys. Chem. B* **2000**, *104*, 3712−3720.
(61) Sitkoff, D.; Sharp, K. A.; Honig, B. Accurate Calculation of Hydration Free Energies Using Macroscopic Solvent Models. *J. Phys. Chem.* **1994**, *98*, 1978−1988.
(62) Pearlman, D. A.; Case, D. A.; Caldwell, J. W.; Ross, W. S.; Cheatham, T. E., III; DeBolt, S.; Ferguson, D.; Seibel, G.; Kollman, P. AMBER, a package of computer programs for applying molecular mechanics, normal mode analysis, molecular dynamics and free energy calculations to simulate the structural and energetic properties of molecules. *Comput. Phys. Commun.* **1995**, *91*, 1−41.
(63) Word, J. M.; Lovell, S. C.; Richardson, J. S.; Richardson, D. C. Asparagine and Glutamine: Using Hydrogen Atom Contacts in the Choice of Side-Chain Amide Orientation. *J. Mol. Biol.* **1999**, *285*, 1735−1747.
(64) Word, J. M.; Lovell, S. C.; LaBean, T. H.; Taylor, H. C.; Zalis, M. E.; Presley, B. K.; Richardson, J. S.; Richardson, D. C. Visualizing and Quantifying Molecular Goodness-of-Fit: Small-Probe Contact Dots with Explicit Hydrogen Atoms. *J. Mol. Biol.* **1999**, *285*, 1711−1733.
(65) Shannon, P.; Markiel, A.; Ozier, O.; Baliga, N. S.; Wang, J. T.; Ramage, D.; Amin, N.; Schwikowski, B.; Ideker, T. Cytoscape: A Software Environment for Integrated Models of Biomolecular Interaction Networks. *Genome Res.* **2003**, *13*, 2498−2504.
(66) Assenov, Y.; Ramírez, F.; Schelhorn, S.-E.; Lengauer, T.; Albrecht, M. Computing Topological Parameters of Biological Networks. *Bioinformatics* **2008**, *24*, 282−284.
(67) Yoon, J.; Blumer, A.; Lee, K. An Algorithm for Modularity Analysis of Directed and Weighted Biological Networks Based on Edge-Betweenness Centrality. *Bioinformatics* **2006**, *22*, 3106−3108.
(68) Freeman, L. C. Centrality in Social Networks Conceptual Clarification. *Social Networks* **1978**, *1*, 215−239.
(69) McCauley, J. A.; McIntyre, C. J.; Rudd, M. T.; Nguyen, K. T.; Romano, J. J.; Butcher, J. W.; Gilbert, K. F.; Bush, K. J.; Holloway, M. K.; Swestock, J.; Wan, B.-L.; Carroll, S. S.; DiMuzio, J. M.; Graham, D. J.; Ludmerer, S. W.; Mao, S.-S.; Stahlhut, M. W.; Fandozzi, C. M.; Trainor, N.; Olsen, D. B.; Vacca, J. P.; Liverton, N. J. Discovery of Vaniprevir (MK-7009), a Macrocyclic Hepatitis C Virus NS3/4a Protease Inhibitor. *J. Med. Chem.* **2010**, *53*, 2443−2463.
(70) Di Paola, L.; De Ruvo, M.; Paci, P.; Santoni, D.; Giuliani, A. Protein Contact Networks: An Emerging Paradigm in Chemistry. *Chem. Rev.* **2012**, *113*, 1598−1613.
(71) Cummings, M. D.; Lindberg, J.; Lin, T.-I.; de Kock, H.; Lenz, O.; Lilja, E.; Felländer, S.; Baraznenok, V.; Nyström, S.; Nilsson, M.; Vrang, L.; Edlund, M.; Rosenquist, Å.; Samuelsson, B.; Raboisson, P.; Simmen, K. Induced-Fit Binding of the Macrocyclic Noncovalent Inhibitor TMC435 to its HCV NS3/NS4A Protease Target. *Angew. Chem., Int. Ed.* **2010**, *49*, 1652−1655.
(72) Vendruscolo, M.; Dokholyan, N. V.; Paci, E.; Karplus, M. Small-World View of the Amino Acids That Play a Key Role in Protein Folding. *Phys. Rev. E* **2002**, *65*, 061910.
(73) Amitai, G.; Shemesh, A.; Sitbon, E.; Shklar, M.; Netanely, D.; Venger, I.; Pietrokovski, S. Network Analysis of Protein Structures Identifies Functional Residues. *J. Mol. Biol.* **2004**, *344*, 1135−1146.
(74) Brinda, K. V.; Vishveshwara, S. A Network Representation of Protein Structures: Implications for Protein Stability. *Biophys. J.* **2005**, *89*, 4159−4170.
(75) Romano, K. P.; Ali, A.; Royer, W. E.; Schiffer, C. A. Drug Resistance against HCV NS3/4A Inhibitors Is Defined by the Balance of Substrate Recognition versus Inhibitor Binding. *Proc. Natl. Acad. Sci* **2010**, *107*, 20986−20991.
(76) Romano, K. P.; Laine, J. M.; Deveau, L. M.; Cao, H.; Massi, F.; Schiffer, C. A. Molecular Mechanisms of Viral and Host-Cell Substrate Recognition by HCV NS3/4A Protease. *J. Virol.* **2011**, *85*, 6106−6116.
(77) Xue, W.; Wang, M.; Jin, X.; Liu, H.; Yao, X. Understanding the Structural and Energetic Basis of Inhibitor and Substrate Bound to the Full-Length NS3/4A: Insights from Molecular Dynamics Simulation, Binding Free Energy Calculation and Network Analysis. *Mol. Biosyst.* **2012**, *8*, 2753−2765.
(78) Wang, J.; Wolf, R. M.; Caldwell, J. W.; Kollman, P. A.; Case, D. A. Development and testing of a general amber force field. *J. Comput. Chem.* **2004**, *25*, 1157−1174.